ACS Catalysis

pubs.acs.org/acscatalysis Letter

Generation of Thioxanthone Hydrogen Anion by Double Photoreduction and Uses for Catalytic Photoreductions

Wen-Jie Kang, Bo Li, Zijian Zhao, Shijie Sun, Changhao Feng, Ke Hu,* K. N. Houk, and Hao Guo*

Cite This: *ACS Catal.* 2023, 13, 13588−13596 Read Online

ACCESS | Metrics & More | Article Recommendations | Supporting Information

ABSTRACT: Anions are the reduced form of precatalysts that are a special type of photoredox catalyst, unlike traditional iridium or ruthenium complexes. Among them, radical anions often have much shorter excited-state lifetimes because of fast nonradiative decay. Herein, we report the discovery of thioxanthone hydrogen anion (**5**), a super-reducing photocatalyst with a long excited-state lifetime (E_{ox}* = −2.74 V vs SCE, τ_S = 4.1 ns). Using **5** as a catalytic reductant, we developed a series of photoreductions, including hydrogenation, reductive dehalogenation, deoxygenative hydrogenation, and deoxygenation, thereby demonstrating the feasibility of the 2e⁻ consecutive photoinduced electron transfer (ConPET) strategy and the versatility of the catalyst.

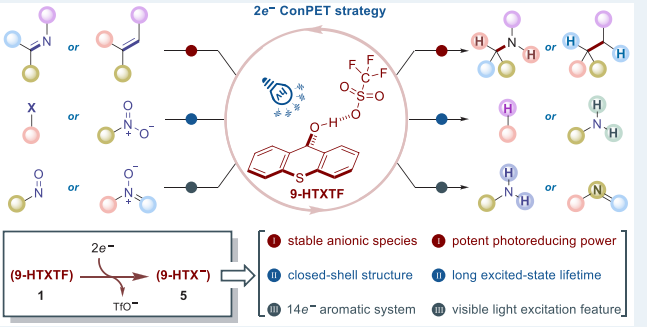

KEYWORDS: *photoredox catalysis, organocatalysis, photoreduction, 2e⁻ ConPET, quantum mechanics calculations*

Photoredox catalysis has revolutionized organic synthesis in recent years,[1] which has provided access to radical intermediates[2] and facilitated redox relay for organometallic intermediates.[3] The redox potential of a photoredox catalyst is a crucial parameter that can be broadened by consecutively absorbing two photons and accumulating multiple-photon energy (Figures 1b,c).[4] The consecutive photoinduced electron transfer (ConPET) process[5] allows the energy-demanding redox transformations, such as dehalogenation and further functionalization,[4,6] alkene oxidation,[7] carboxylation,[8] arene oxidation,[9] Birch reduction,[10] and N−O bond cleavage,[11] under mild conditions.[12] While excited-state lifetime is another important feature of photoredox catalysts, open-shell intermediates, such as radical anions[13] or radical cations[14] generated by one-electron transfer of precatalysts, often have significantly shorter excited-state lifetimes because of fast nonradiative decay. Recently, closed-shell catalytic intermediates[15] produced by two-electron reduction of precatalysts have been reported, which possess relatively longer excited-state lifetimes (nanosecond time scale) and promising application to several photoredox reactions (Figure 1a).[16] However, related reactions have been rarely reported. Therefore, we propose a 2e⁻ ConPET strategy that combines the advantages of the long excited-state lifetime of two-electron reduced catalysts[16] and the broad redox window of known ConPET processes,[4] which offers a platform for the development of new synthetic methodologies and the expansion of catalyst applications (Figure 1d). In this context, we report the discovery, characterization, and reactivity of thioxanthone hydrogen anion **5**, a closed-shell photoreductant with a long excited-state lifetime (E_{ox}* = −2.74 V vs SCE, τ_S = 4.1 ns) that is accessed via double photoreduction of **1**. Importantly, its reductive capability is stronger than those of other anionic [NMI(H)⁻] and dianionic (PDI^{2-}) photocatalysts. Using **5** as a catalytic reductant, we developed a series of photoreductions, including the hydrogenation of imines and alkenes, reductive dehalogenation of halides, deoxygenative hydrogenation of nitro and nitroso compounds, and deoxygenation of *N*-oxides, thereby demonstrating the versatility and potential of this intermediate in the development of new synthetic methodologies and the expansion of catalyst applications (Figure 1e).

In our previous work,[17] **2** was identified as a potent and long-lived photooxidant, albeit with limited reduction potential because of the poor electron-donating ability of *p*-xylene. With continued interest in this field, we conducted a comprehensive study of the reduced species of **1**, which held the potential to function as a robust reductant (Figure 2a). Cyclic voltammetry (CV) measurements indicated that thioxanthone (**TX**) underwent a perfectly reversible one-electron reduction process to result in the formation of the radical anion $\mathbf{TX}^{\bullet-}$, as previously observed (Figure 2b, green). Further expansion of the scan range revealed an electrochemically irreversible reduction event for **TX**, which corresponded to a two-electron transfer process that generated the dianions $\mathbf{TX}^{2-}$ (Figure 2b, blue).

Received: August 23, 2023
Revised: October 3, 2023
Published: October 9, 2023

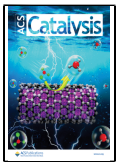

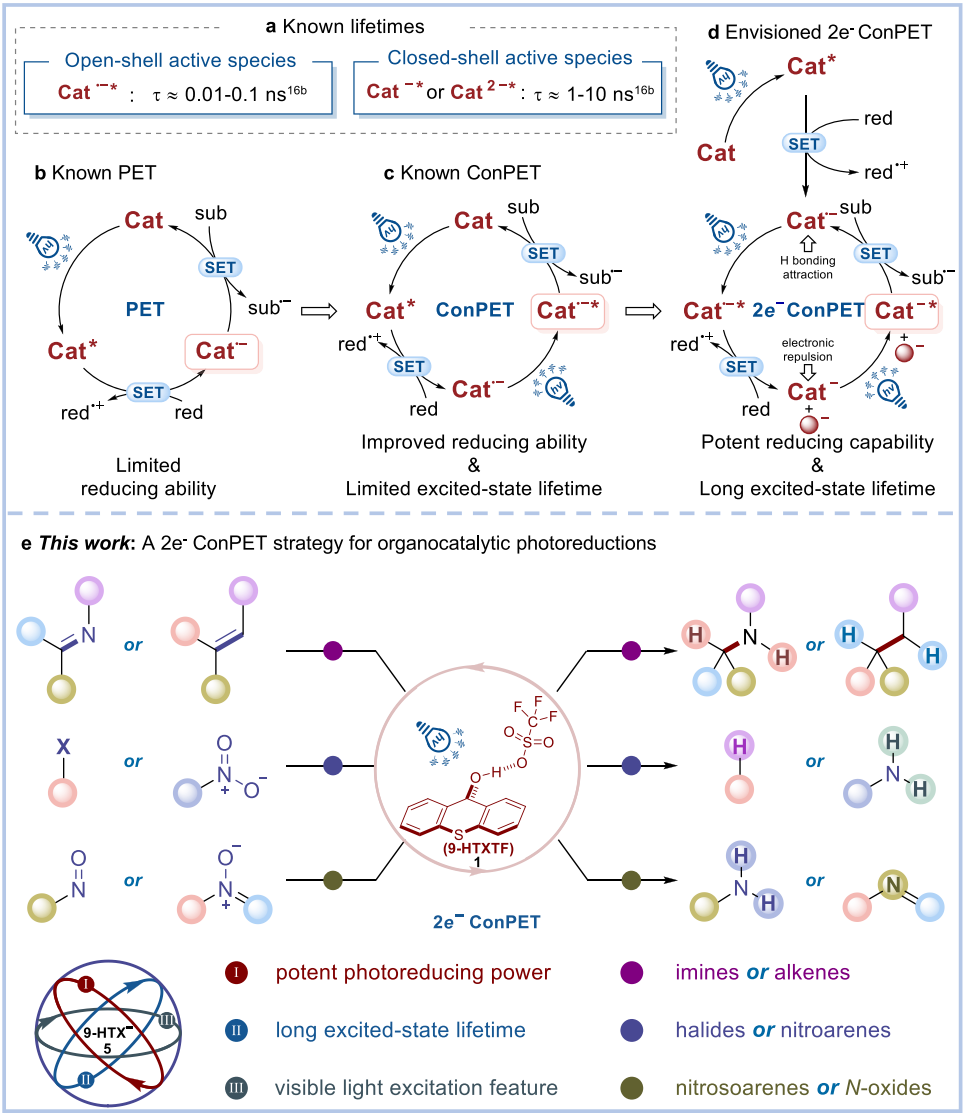

Figure 1. Reaction design. (a) Known lifetimes. (b) Known PET strategy. (c) Known ConPET strategy. (d) Envisioned 2e⁻ ConPET strategy. (e) This work: a 2e⁻ ConPET strategy for organocatalytic photoreductions. Cat, catalyst; red, reductant; sub, substrate.

Additionally, CV of **1** showed an irreversible oxidative feature and a reductive peak (Figure 2b, red), thereby corresponding well to the irreversible wave of **TX**. These results led us to speculate that the reduced state of **1** was not a one-electron reduced open-shell molecule but a two-electron reduced closed-shell species consistent with recent reports on two-electron reducing species.[16a,18] Differential pulse voltammetry (DPV) experiments of **TX** and **1** were performed and analyzed together with the CV of **TX** and **1** (Figure 2c). These data further demonstrated that the two-electron reduced state of **TX** (i.e., $\mathbf{TX}^{2-}$) was generated by $1e^-$ manifolds, while that of **1** was yielded by $2e^-$ manifolds,[18] thereby exhibiting completely different electrochemical properties. To confirm the structure and photophysical properties of the reduced state of **1**, we applied a reducing agent and light to obtain the reduced species. Our results showed that the bright yellow **1** solution turned yellow upon irradiation by 415 nm LEDs with the addition of PPh_3, which indicated the formation of a new species (Figure 2a). UV−vis spectroscopy, UV−vis spectroelectrochemistry, and dynamic UV−vis analysis revealed a significant change in the absorption band after undergoing photoreduction or electroreduction, which confirmed the formation of new species (Figures 2d−f). Subsequent ^{1}H NMR analysis showed the formation of a new set of peaks with irradiation time extension (Figure 2g). Meanwhile, no electron paramagnetic resonance (EPR) signals were detected (Figure S6), thereby supporting the conclusion that the reduced species is a diamagnetic closed-shell species. The newly emerged H signals can be assigned to the aromatic hydrogens. No nonaromatic hydrogen appeared, and the aromatic hydrogens dramatically upfield shifted, which indicated that the two-electron reduced species of **1** was **5** (Figures 2g and S3). Meanwhile, theoretical calculations showed that anionic species **5** mainly exists without the association of TfO^- to avoid electronic repulsion (Figure 2g, $\Delta G_{diss} = -6.4$ kcal/mol), and the electrons of the carbanion in **5** were well delocalized to the two benzene rings, thus maintaining a stable anionic structure (Figure 2j). The 14-electron tricyclic system of **5** ensures the aromaticity of the whole molecule and its excitation by visible light. Control experiments indicated that light, TfOH, and PPh_3 were all necessary for the formation of **5** (Figures S3−5). Notably, photoexcitation of **5** led to a new

https://doi.org/10.1021/acscatal.3c03972
ACS Catal. 2023, 13, 13588−13596

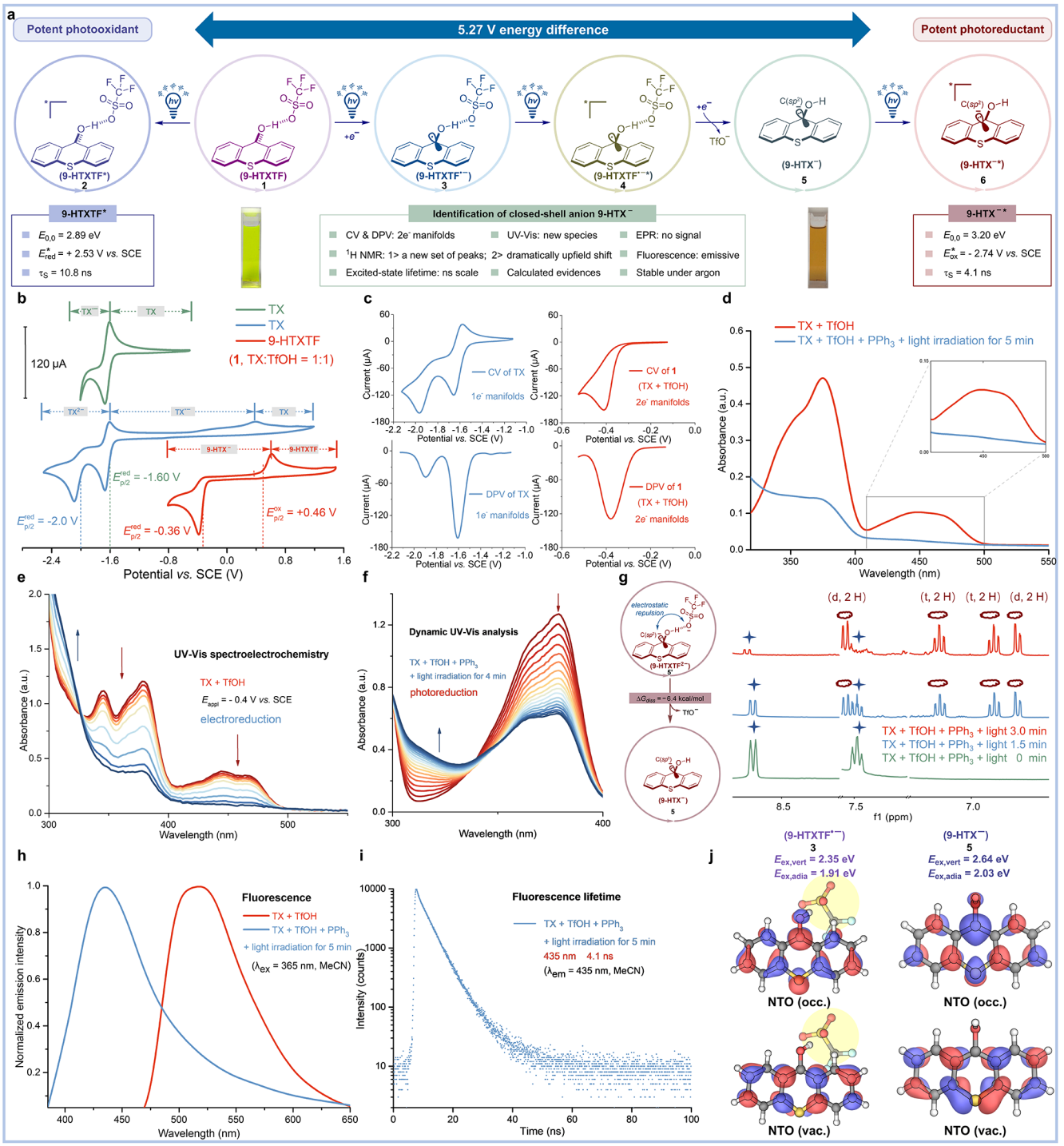

Figure 2. Properties of the emissive closed-shell anion **5**. (a) Light-driven formation of **5**. (b) Cyclic voltammetry; for details, see the Supporting Information. (c) Cyclic voltammetry and differential pulse voltammetry of **TX** and **1** in MeCN (0.1 M TBAP). (d) Absorbance profiles for **1** [**TX** (0.1 mM) and TfOH (0.1 mM)] and **5** [**TX** (0.1 mM), TfOH (0.1 mM), PPh_3 (0.3 mM), and light (5 min)] in MeCN. (e) UV−vis spectroelectrochemistry of **1** in MeCN (0.1 M TBAP) with an applied bias of −0.4 V vs SCE. (f) A solution of **TX** (200 μM), TfOH (400 μM), and PPh_3 (2 mM) in MeCN (2 mL) was irradiated by 405 nm laser irradiation (0.3 W/cm^2) at rt under an argon atmosphere for 4 min. (g) ^{1}H NMR spectra (400 MHz, $CDCl_3$), for details, see the Supporting Information. (h) Fluorescence emission spectra (λ_{ex} = 365 nm) of **1** [**TX** (0.1 mM) and TfOH (0.1 mM)] and **5** [**TX** (0.1 mM), TfOH (0.1 mM), PPh_3 (0.3 mM) and light (5 min)] collected in MeCN. (i) Fluorescence lifetime profiles for **5** [**TX** (0.1 mM), TfOH (0.1 mM), PPh_3 (0.3 mM) and light (5 min)] in MeCN. (j) Excitation energies and visualization of natural transition orbitals (NTOs). Calculations were performed at the level of (TD-) CAM-B3LYP/def2-TZVP/SMD(CH_3CN). ex, excitation; em, emission; MeCN, acetonitrile; and TBAP, tetrabutylammonium perchlorate.

fluorescence emission peak (λ_{em} = 435 nm), and its corresponding lifetime was measured to be 4.1 ns (Figures 2h,i). The calculations further showed that **5** shares a comparable first excitation energy with **3** (Figure 2j), which can be ascribed to a $\pi-\pi^*$ excitation mode, thereby indicating that the potent reductive power of **5** results from its extra

https://doi.org/10.1021/acscatal.3c03972
ACS Catal. 2023, 13, 13588−13596

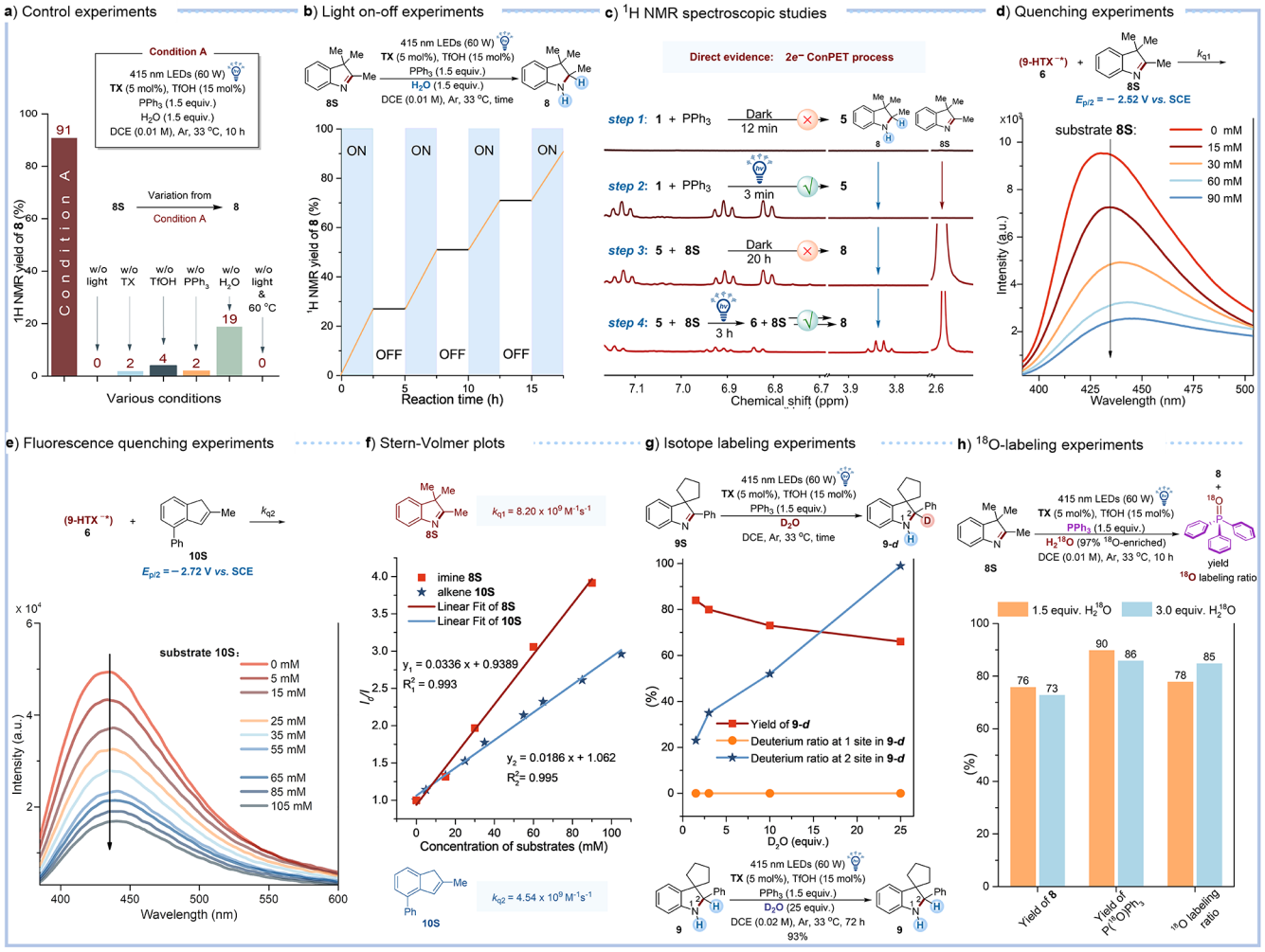

Figure 3. Mechanism studies. (a) Control experiments. (b) Light on−off experiments. (c) ^{1}H NMR spectroscopic studies. (d−f) Stern−Volmer fluorescence quenching experiments. (g) Isotope labeling experiments. Isolated yields were reported, and deuterium ratios were determined by ^{1}H NMR analysis. (h) ^{18}O-Labeling experiments. Isolated yields were reported, and the ^{18}O-labeling ratios were determined by HRMS analysis. For mechanistic study details, see the Supporting Information. $E_{p/2}$, half-peak potential.

electron occupation. Ultimately, the theoretical excited-state oxidation potential of **5** was calculated to be −2.74 V vs SCE by combining the absorbance profile, emission spectrum, and CV results (for details, see the Supporting Information). Notably, its reductive capability is stronger than that of recently reported two-electron reduced closed-shell photocatalysts {E_{ox} [NMI(H)$^{-}$*] = −2.63 V vs SCE, E_{ox} (PDI^{2-}*) = −2.65 V vs SCE, NMI = naphthlalene monoimide, PDI = perylene diimide}.[16] These results suggested that **5** might serve as a new super-reducing photocatalyst with sufficiently long excited-state lifetime.

With the characterization of the photophysical and electrochemical properties of **5**, our aim was to employ this species as a photocatalytic reductant for multielectron reactions. In our previous work,[17] alkene hydrogenation was achieved using 1-methylquinolin-2(1*H*)-one ($E_{p/2}$ = −2.10 V vs SCE) as the standard substrate. Given the long excited-state lifetime and potent photoreducing power of **5**, we selected here the more challenging 2,3,3-trimethyl-3*H*-indole (**8S**, $E_{p/2}$ = −2.52 V vs SCE) as the initial model for imine hydrogenation to investigate in detail. Following the optimization of this reaction, condition A was developed [Figure 3a; **TX** (5 mol %), TfOH (15 mol %), PPh_3 (1.5 equiv), and H_2O (1.5 equiv) in DCE (0.01 M) under the irradiation of 415 nm LEDs at 33 °C].

Control experiments revealed that all components of the reaction conditions were critical (Figure 3a). With regard to the 19% yield attained without the addition of H_2O, we hypothesized that the inevitable trace amounts of H_2O in the reaction system resulted in product formation. The absence of light at 60 °C caused no reaction, which indicated that the reaction is unlikely to be driven thermally under the conditions employed. To gain a comprehensive understanding of the reaction mechanism, light on−off experiments were performed (Figure 3b). The formation or cessation of product occurred immediately upon switching on or off the irradiation. Moreover, the overall quantum yield of the model reaction was 0.13 in DCE and 0.0019 in MeCN (Figure S8). Taken together, we did not find support for a radical chain mechanism. Control experiments, light on−off experiments, and the overall quantum yield strongly suggested that imine hydrogenation was a photoinduced electron transfer (PET) reaction. Importantly, ^{1}H NMR spectroscopic studies confirmed the 2e^{-} ConPET process (Figures 3c and S9). Excitation of **1** allowed the formation of **5** (Figure 3c, steps 1 and 2), which was otherwise forbidden. Notably, in the

https://doi.org/10.1021/acscatal.3c03972
ACS Catal. 2023, 13, 13588−13596

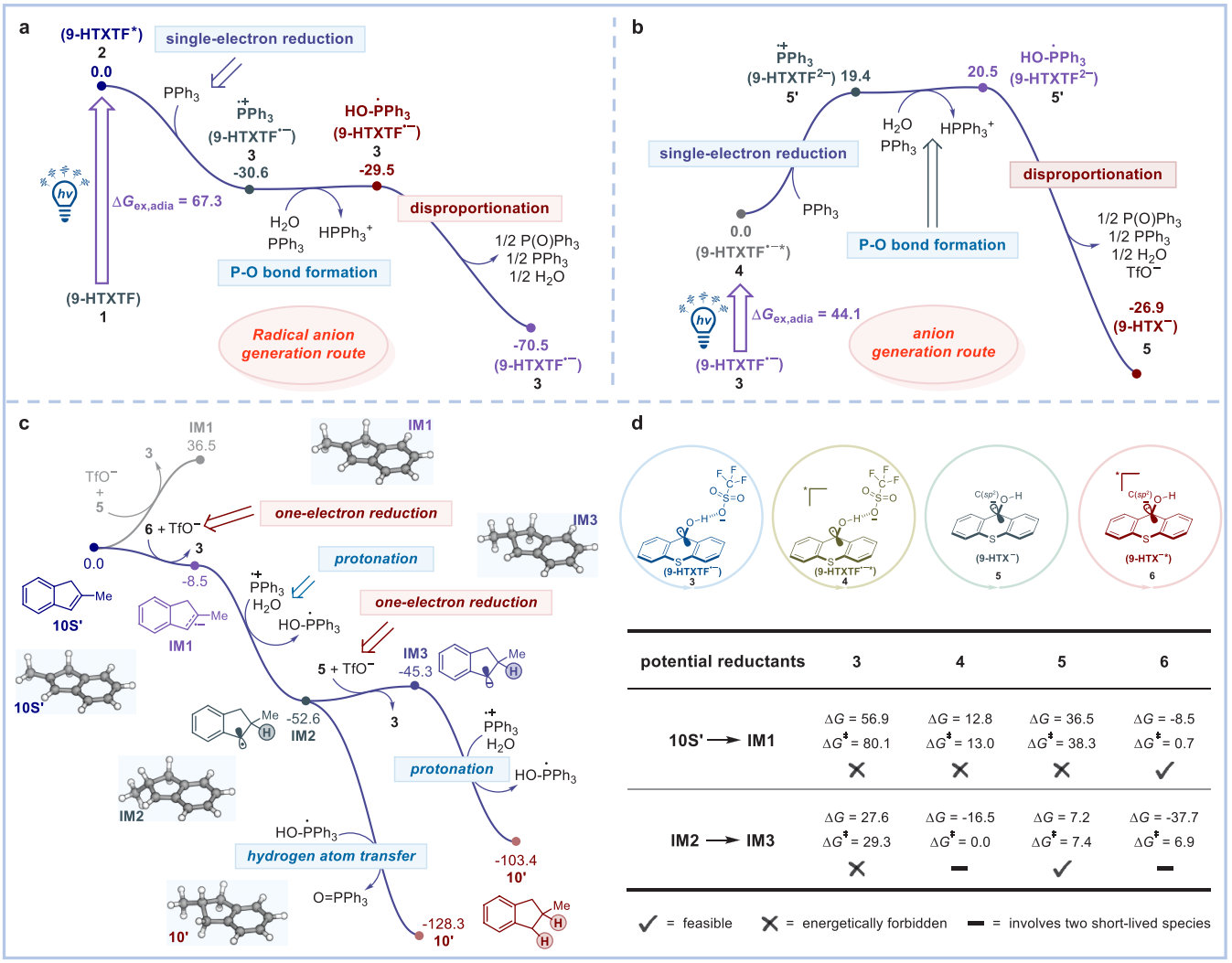

Figure 4. Density functional theory (DFT) calculations and the proposed mechanism. Free-energy profiles for the formations of (a) **3** and (b) **5** (unit: kcal/mol). Calculated free energy profile for the photocatalytic hydrogenation of **10S′** (c,d) comparative studies on the possible anionic reactants. All energies are in kcal/mol. Calculations were performed at the level of (TD-) CAM-B3LYP/def2-TZVP/SMD(CH_3CN). For details, see the Supporting Information.

absence of light, **5** was stable under an argon atmosphere for at least 7 days (Figure S9) but was incapable of reducing **8S** (Figure 3c, step 3). Following 7 days, long-lived **5** was excited again by light irradiation to produce **6**, which was then quenched by **8S** to yield the hydrogenation product **8** (Figure 3c, step 4). Stern−Volmer fluorescence quenching experiments showed that the excited state of **1** could be quenched by PPh_3 (Figure S10), which is obvious proof for the first PET. Furthermore, generated **6** could be quenched by imine **8S** ($E_{p/2}$ = −2.52 V vs SCE, Figure 3d) or unactivated alkene **10S** ($E_{p/2}$ = −2.72 V vs SCE, Figure 3e). The Stern−Volmer plots in Figure 3f displayed a linear photoluminescence intensity quenching of **6** by **8S** or **10S**, with quenching rate constants of $k_{q1} = 8.20 \times 10^9\ M^{-1}\ s^{-1}$ and $k_{q2} = 4.54 \times 10^9\ M^{-1}\ s^{-1}$, which further affirmed the ConPET process in this catalytic cycle. Isotope labeling experiments were then conducted to determine the hydrogen source of this reaction (Figure 3g). The addition of 1.5 equiv of D_2O led to only partial deuterium ratio, likely because of trace amounts of H_2O in the reaction mixture. With increasing D_2O content, the deuterium ratio at the 2 site in **9-*d*** correspondingly increased. Upon the addition of 25 equiv of D_2O, the deuterium ratio at the 2 site in **9-*d*** reached 99% (Figure 3g). These results conclusively affirmed that (1) hydrogen originated from H_2O and (2) hydrogen participated in this reaction in the form of a proton. Additionally, hydrogenated product **9** was applied under condition A in the presence of 25 equiv of D_2O. The result revealed that product **9** was not deuterated at all (Figure 3g), thereby indicating that the deuterium was introduced into the product during the reaction process. Ultimately, the ^{18}O-labeling experiments with $H_2{}^{18}O$ in which PPh_3 conversion to $^{18}O{=}PPh_3$ was observed clearly indicated that PPh_3 was the sacrificial electron donor and mediated the chemical activation of water (Figure 3h).

Quantum mechanical calculations confirmed the formation of **3** and **5**. As displayed in Figure 4a, the photoexcited **2** is readily reduced by Ph_3P to yield radical species **3** with a rather negative ΔG (−30.6 kcal/mol). Meanwhile, the resulting $Ph_3P^{\bullet+}$ might entail formation of $[HO{-}PPh_3]^{\bullet}$ and the irreversible disproportion thereof toward 1/2 $O{=}PPh_3$, 1/2 PPh_3, and 1/2 H_2O,[19] which gives rise to a ΔG_{tot} of −70.5 kcal/mol. Subsequently, as described in Figure 4b, the photoexcitation of radical species **3** allowed the resultant **4** to undergo the second reduction by PPh_3. Despite a positive

https://doi.org/10.1021/acscatal.3c03972
ACS Catal. 2023, 13, 13588−13596

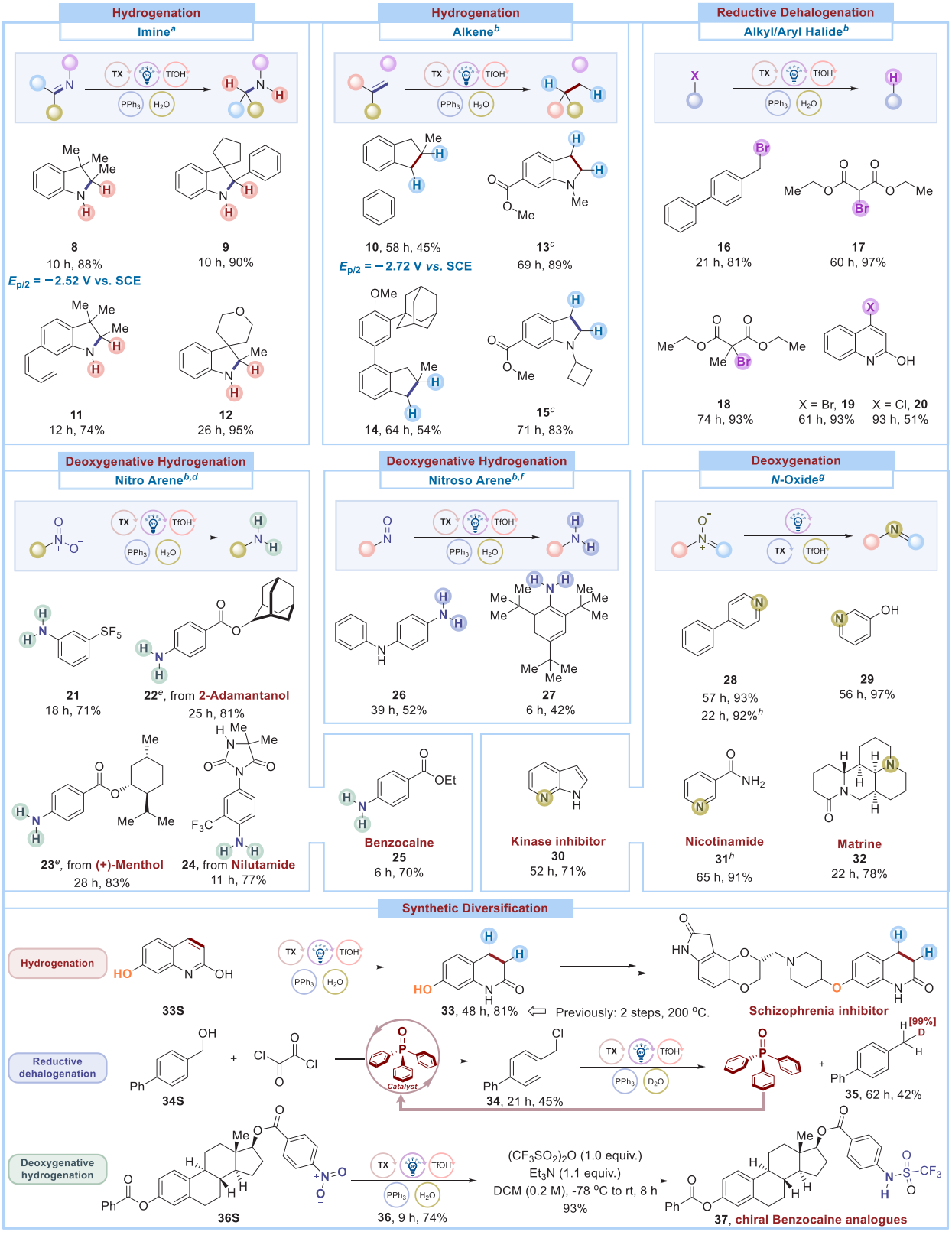

Figure 5. Photocatalytic reductions of imines, alkenes, halides, nitroarenes, nitrosoarenes, and *N*-oxides, as well as synthetic diversification. [a]Condition A: **S** (0.1 mmol), **TX** (5 mol %), TfOH (15 mol %), PPh_3 (1.5 equiv), and H_2O (1.5 equiv) in anhydrous DCE (c = 0.01 M) were irradiated by 415 nm LEDs (60 W) at 33 °C under argon atmosphere. Isolated yield was reported. [b]Condition B: **S** (0.2 mmol), **TX** (2.5 mol %), TfOH (5 mol %), PPh_3 (1.1 equiv), and H_2O (1.5 equiv) in anhydrous MeCN (c = 0.02 M) were irradiated by 415 nm LEDs (60 W) at 33 °C under argon atmosphere. [c]**TX** (10 mol %), TfOH (1.0 equiv), and PPh_3 (1.5 equiv) were used. [d]PPh_3 (3.5 equiv) was used. [e]Performed at the 0.1 mmol scale. [f]PPh_3 (2.5 equiv) was used. [g]Condition C: **S** (0.2 mmol), **TX** (2.5 mol %), and TfOH (5 mol %) in anhydrous MeCN (c = 0.02 M) were irradiated by 415 nm LEDs (60 W) at 33 °C under an argon atmosphere. [h]**TX** (10 mol %) and TfOH (20 mol %) were used. For synthetic diversification details,[20] see the Supporting Information. $E_{p/2}$, half-peak potential. Note: 60 W LEDs were used for nine parallel photoreactions.

https://doi.org/10.1021/acscatal.3c03972
ACS Catal. 2023, 13, 13588−13596

ΔG of 19.4 kcal/mol for the one-electron reduction, the disproportionation can analogously take place in an irreversible manner to drive the equilibrium toward **5**. The calculations further suggested that photoinduced reductions of **1** and **3** by PPh_3 were both spontaneous, thus strengthening the proposed $2e^-$ ConPET strategy.

Considering that the reduction potential of **10S** is −2.72 V vs SCE, its catalytic hydrogenation is extremely challenging. However, Stern−Volmer luminescence quenching experiments foreboded that **6** was able to reduce **10S** (Figure 3e). Therefore, **10S′** was chosen as the computation model to explore the role of **6** in the catalytic hydrogenation in order to provide insightful guidance for the following research. Figure 4c exhibits the calculated free energy profile, which involves two cycles of the reduction−protonation cascade to achieve the hydrogenation. The process commences with the one-electron reduction of **10S′** by **6** to form radical anionic intermediate **IM1** (ΔG = −8.5 kcal/mol). Reduction by **5** would require a much higher ΔG of 36.5 kcal/mol to achieve the same reduction, thereby highlighting the exceptional reducing ability of **6**. These computational results were consistent with the experimental findings from ^{1}H NMR spectroscopic studies of the $2e^-$ ConPET process, Stern−Volmer luminescence quenching experiments of **6**, and cyclic voltammetry measurement of substrates [i.e., excited **6** can reduce these substrates; E_{ox} (**6**) = −2.74 V vs SCE < $E_{p/2,\ red}$ (substrates); for CV details of substrates, see the Supporting Information]. The protonation of **IM1** leads to the formation of benzylic radical **IM2**, which can accept an electron from **5** to generate a highly basic benzylic carbanion **IM3**. The product **10′** can be readily formed via a final protonation step. Alternatively, **10′** might also be formed via the direct hydrogen atom transfer (HAT) from $[HO{-}PPh_3]^\bullet$ to **IM2**. Both pathways appear energetically feasible and might contribute to the reaction depending on multiple factors, such as substrate type.

A feature of the present catalytic system is the involvement of multiple anionic reducing species derived from **1**. We studied potential anionic reductants for the reduction of **10S′** and the radical intermediate **IM2** and performed combined kinetic and thermodynamic analyses, as summarized in Figure 4d. The calculations reveal that the reduction of **10S′** is exclusively feasible with the most potent reducing agent, **6**. However, for the reduction of radical **IM2**, the computations suggest that **4**, **5**, and **6** all exhibit feasible energetics. In consideration that the reduction of **IM2** by **4** or **6** would require the excited-state species to encounter a radical intermediate in solution, we presume that ground-state species **5** is the primary reductant for **IM2** in the reaction. These theoretical findings suggest that our photocatalytic system may dynamically self-select the optimal redox mode to match multiple target species covering a range of potentials. This is expected to broaden the applicability of our approach to diverse substrate classes and reaction pathways.

Motivated by the insight that multiple reducing species are generated in the $2e^-$ ConPET process, we conducted a thorough investigation into the universality of this catalytic system for different types of multielectron reactions. Through persistent efforts, we successfully achieved hydrogenation, reductive dehalogenation, and deoxygenative hydrogenation reactions, as demonstrated in Figure 5 (for control experiments, see Tables S7−9). We selected representative substrates to demonstrate the feasibility of the $2e^-$ ConPET strategy and the versatility of the catalyst. In the hydrogenation of imines, various cyclic imines with different electronic effects afforded the corresponding hydrogenation products in good to excellent yields (**8**, **11**, and **12**). 2-Aryl-substituted 3*H*-indole could also be hydrogenated to give desired product **9**. Different ring-substituted substrates were also competent and successfully delivered hydrogenated products in excellent yields (**9** and **12**). In the hydrogenation of alkenes, both unactivated alkenes (**10** and **14**) and electron-rich alkenes (**13**−**15**) could deliver the desired products in moderate to good yields. Compared with our previous work,[17] the photocatalyst shows a more potent reductive power, which results in the reduction of electron-rich or unactivated alkenes. In the reductive dehalogenation reaction, both alkyl halides (**16**−**18**) and aryl halides (**19** and **20**) were successfully transformed to the corresponding hydrodebrominated or hydrodechlorinated products under optimized conditions. By treating commercialized ethyl 4-nitrobenzoate under improved optimal conditions, we obtained a local anesthetic, benzocaine (**25**), while nitroarene with an electronically differentiated substitute was also amenable to the reaction conditions (**21**). Moreover, we were able to synthesize medicinally interesting benzocaine analogues in good yields by modifying 4-nitrobenzoic acid with adamantanol and menthol motifs (**22** and **23**). The late-stage deoxygenative hydrogenation of nilutamide, an antiandrogen drug used primarily for the treatment of prostate cancer, efficiently yielded product **24**. The preferential reduction of the nitro group over the trifluoromethyl group can be attributed to the limited distribution of the lowest unoccupied molecular orbital (LUMO) on the trifluoromethyl group (Figure S11). In the deoxygenative hydrogenation of nitrosoarenes, different substituted aniline analogues (**26** and **27**) were obtained under modified optimized conditions.

On the basis of our previous investigations, we sought to explore the potential of our catalyst for deoxygenation reactions. By removing the hydrogen source and reducing agent from condition B, we achieved the metal-free deoxygenation of *N*-oxides (for control experiments, see Table S10). This finding is particularly significant for organic synthesis since the solvent can also serve as a reductant, which avoids the need for large quantities of organic or inorganic reducing agents. Notably, we observed that the reaction was significantly expedited with a higher catalyst loading (**28**). Representative examples are listed in Figure 5. In the deoxygenation of pyridine-*N*-oxides, various medicinally relevant pyridine products were directly synthesized in good yields (**28**-**30**). Nicotinamide (**31**), which exhibits a protective effect against pellagra, was obtained in excellent yield using the condition C. Commercially available oxymatrine could be efficiently converted into matrine (**32**), a plant insecticide drug, via a similar deoxygenation process, while preserving the stereocenters. Notably, the completely metal-free photochemical reduction platforms, including hydrogenation, reductive dehalogenation, deoxygenative hydrogenation, and deoxygenation, provide new avenues for achieving synthetically valuable transformations. For example, the hydrogenation of **33S** generated **33**, which can be used to obtain schizophrenia inhibitors using known methods.[20] Chlorination of alcohol **34S** catalyzed by triphenylphosphine oxide ($O{=}PPh_3$), followed by a reductive dehalogenation reaction, afforded monodeuterium-labeled product **35** with an excellent deuterium ratio and $O{=}PPh_3$, which can be used as a catalyst in the entire transformation procedure. It is important to note that chiral

https://doi.org/10.1021/acscatal.3c03972
ACS Catal. 2023, 13, 13588−13596

benzocaine analogues **37** were obtained via deoxygenative hydrogenation of the chiral nitroaromatic **36S** and subsequent amino protection.

In summary, the present study demonstrates that the closed-shell anionic species **5**, obtained by the two-electron reduction of **1**, exhibits remarkable photocatalytic activity with prolonged excited-state lifetime. The highly potent excited **6** enables a wide range of reduction reactions, including imines, alkenes, halides, nitroarenes, nitrosoarenes, and *N*-oxides, which underscores the versatility of the catalyst and the universality of the substrate scope. The chemical activation of water as a green and sustainable hydrogen source in the aforementioned hydrogenation-related reactions is notable and represents an ideal method to convert earth-abundant sources into high-value chemicals. Moreover, the solvent acts as a reductant in deoxygenation reaction (i.e., reduction of *N*-oxides), thereby avoiding the dependence on organic or inorganic reducing agents. These metal-free catalytic systems open up new possibilities for the synthesis of high-value-added drugs and bioactive molecules, and the $2e^-$ ConPET strategy offers a platform for the development of new synthetic methodologies and the expansion of catalyst applications.

■ ASSOCIATED CONTENT

Supporting Information

The Supporting Information is available free of charge at https://pubs.acs.org/doi/10.1021/acscatal.3c03972.

Additional experimental details, characterization, and spectra (PDF)

■ AUTHOR INFORMATION

Corresponding Authors

Ke Hu − *Department of Chemistry, Fudan University, Shanghai 200438, P. R. China;* orcid.org/0000-0002-0240-7192; Email: khu@fudan.edu.cn

Hao Guo − *Department of Chemistry, Fudan University, Shanghai 200438, P. R. China;* orcid.org/0000-0003-3314-4564; Email: Hao_Guo@fudan.edu.cn

Authors

Wen-Jie Kang − *Department of Chemistry, Fudan University, Shanghai 200438, P. R. China*

Bo Li − *Department of Chemistry and Biochemistry, University of California, Los Angeles, California 90095, United States*

Zijian Zhao − *Department of Chemistry, Fudan University, Shanghai 200438, P. R. China*

Shijie Sun − *Department of Chemistry, Fudan University, Shanghai 200438, P. R. China*

Changhao Feng − *Department of Chemistry, Fudan University, Shanghai 200438, P. R. China*

K. N. Houk − *Department of Chemistry and Biochemistry, University of California, Los Angeles, California 90095, United States;* orcid.org/0000-0002-8387-5261

Complete contact information is available at: https://pubs.acs.org/10.1021/acscatal.3c03972

Notes

The authors declare no competing financial interest.

■ ACKNOWLEDGMENTS

We acknowledge the Shanghai Science and Technology Committee (21JM0010600 to H.G.) and the National Institute of General Medical Sciences of the NIH (R01GM124480 to K.N.H.) for financial support. We are grateful to Prof. Ming Gong and Prof. Haoyang Wang for valuable discussions. We thank Xiaoya Zhao and Junyi Wang for providing fluorescence and phosphorescence spectrophotometers.

■ REFERENCES

(1) (a) Reed, N. L.; Yoon, T. P. Oxidase reactions in photoredox catalysis. *Chem. Soc. Rev.* **2021**, *50*, 2954−2967. (b) Chan, A. Y.; Perry, I. B.; Bissonnette, N. B.; Buksh, B. F.; Edwards, G. A.; Frye, L. I.; Garry, O. L.; Lavagnino, M. N.; Li, B. X.; Liang, Y.; Mao, E.; Millet, A.; Oakley, J. V.; Reed, N. L.; Sakai, H. A.; Seath, C. P.; MacMillan, D. W. C. Metallaphotoredox: The Merger of Photoredox and Transition Metal Catalysis. *Chem. Rev.* **2022**, *122*, 1485−1542. (c) Allen, A. R.; Noten, E. A.; Stephenson, C. R. J. Aryl Transfer Strategies Mediated by Photoinduced Electron Transfer. *Chem. Rev.* **2022**, *122*, 2695−2751. (d) Candish, L.; Collins, K. D.; Cook, G. C.; Douglas, J. J.; Gomez-Suarez, A.; Jolit, A.; Keess, S. Photocatalysis in the Life Science Industry. *Chem. Rev.* **2022**, *122*, 2907−2980.

(2) Pitre, S. P.; Overman, L. E. Strategic Use of Visible-Light Photoredox Catalysis in Natural Product Synthesis. *Chem. Rev.* **2022**, *122*, 1717−1751.

(3) Holmberg-Douglas, N.; Nicewicz, D. A. Photoredox-Catalyzed C−H Functionalization Reactions. *Chem. Rev.* **2022**, *122*, 1925−2016.

(4) (a) Ghosh, I.; Ghosh, T.; Bardagi, J. I.; König, B. Reduction of aryl halides by consecutive visible light-induced electron transfer processes. *Science* **2014**, *346*, 725−728. (b) MacKenzie, I. A.; Wang, L.; Onuska, N. P. R.; Williams, O. F.; Begam, K.; Moran, A. M.; Dunietz, B. D.; Nicewicz, D. A. Discovery and characterization of an acridine radical photoreductant. *Nature* **2020**, *580*, 76−80.

(5) (a) Baek, Y.; Reinhold, A.; Tian, L.; Jeffrey, P. D.; Scholes, G. D.; Knowles, R. R. Singly Reduced Iridium Chromophores: Synthesis, Characterization, and Photochemistry. *J. Am. Chem. Soc.* **2023**, *145*, 12499−12508. (b) Horsewill, S. J.; Hierlmeier, G.; Farasat, Z.; Barham, J. P.; Scott, D. J. Shining Fresh Light on Complex Photoredox Mechanisms through Isolation of Intermediate Radical Anions. *ACS Catal.* **2023**, *13*, 9392−9403.

(6) (a) Zeng, L.; Liu, T.; He, C.; Shi, D.; Zhang, F.; Duan, C. Organized Aggregation Makes Insoluble Perylene Diimide Efficient for the Reduction of Aryl Halides via Consecutive Visible Light-Induced Electron-Transfer Processes. *J. Am. Chem. Soc.* **2016**, *138*, 3958−3961. (b) Ghosh, I.; König, B. Chromoselective Photocatalysis: Controlled Bond Activation through Light-Color Regulation of Redox Potentials. *Angew. Chem., Int. Ed.* **2016**, *55*, 7676−7679. (c) Neumeier, M.; Sampedro, D.; Májek, M.; de la Peña O'Shea, V. A.; Jacobi von Wangelin, A.; Pérez-Ruiz, R. Dichromatic Photocatalytic Substitutions of Aryl Halides with a Small Organic Dye. *Chem.—Eur. J.* **2018**, *24*, 105−108. (d) Connell, T. U.; Fraser, C. L.; Czyz, M. L.; Smith, Z. M.; Hayne, D. J.; Doeven, E. H.; Agugiaro, J.; Wilson, D. J. D.; Adcock, J. L.; Scully, A. D.; Gómez, D. E.; Barnett, N. W.; Polyzos, A.; Francis, P. S. The Tandem Photoredox Catalysis Mechanism of $[Ir(ppy)_2(dtb\text{-}bpy)]^+$ Enabling Access to Energy Demanding Organic Substrates. *J. Am. Chem. Soc.* **2019**, *141*, 17646−17658. (e) Kerzig, C.; Guo, X.; Wenger, O. S. Unexpected Hydrated Electron Source for Preparative Visible-Light Driven Photoredox Catalysis. *J. Am. Chem. Soc.* **2019**, *141*, 2122−2127. (f) Giedyk, M.; Narobe, R.; Weiß, S.; Touraud, D.; Kunz, W.; König, B. Photocatalytic activation of alkyl chlorides by assembly-promoted single electron transfer in microheterogeneous solutions. *Nat. Catal.* **2020**, *3*, 40−47. (g) Forni, J. A.; Micic, N.; Connell, T. U.; Weragoda, G.; Polyzos, A. Tandem Photoredox Catalysis: Enabling Carbonylative Amidation of Aryl and Alkylhalides. *Angew. Chem., Int. Ed.* **2020**, *59*, 18646−18654. (h) Chmiel, A. F.; Williams, O. P.; Chernowsky, C. P.; Yeung, C. S.; Wickens, Z. K. Non-innocent Radical Ion Intermediates in Photoredox Catalysis: Parallel Reduction Modes Enable Coupling of Diverse Aryl Chlorides. *J. Am. Chem. Soc.* **2021**, *143*, 10882−10889. (i) Xu, J.; Cao, J.; Wu, X.; Wang, H.; Yang, X.; Tang, X.; Toh, R. W.; Zhou, R.; Yeow, E. K. L.; Wu, J. Unveiling Extreme Photoreduction Potentials of Donor-

Acceptor Cyanoarenes to Access Aryl Radicals from Aryl Chlorides. *J. Am. Chem. Soc.* **2021**, *143*, 13266−13273. (j) Widness, J. K.; Enny, D. G.; McFarlane-Connelly, K. S.; Miedenbauer, M. T.; Krauss, T. D.; Weix, D. J. CdS Quantum Dots as Potent Photoreductants for Organic Chemistry Enabled by Auger Processes. *J. Am. Chem. Soc.* **2022**, *144*, 12229−12246. (k) Zhao, Z.; Niu, F.; Li, P.; Wang, H.; Zhang, Z.; Meyer, G. J.; Hu, K. Visible Light Generation of a Microsecond Long-Lived Potent Reducing Agent. *J. Am. Chem. Soc.* **2022**, *144*, 7043−7047.

(7) Rombach, D.; Wagenknecht, H.-A. Photoredox Catalytic Activation of Sulfur Hexafluoride for Pentafluorosulfanylation of α-Methyl- and α-Phenyl Styrene. *ChemCatChem.* **2018**, *10*, 2955−2961.

(8) (a) Song, L.; Wang, W.; Yue, J.-P.; Jiang, Y.-X.; Wei, M.-K.; Zhang, H.-P.; Yan, S.-S.; Liao, L.-L.; Yu, D.-G. Visible-light photocatalytic di- and hydro-carboxylation of unactivated alkenes with CO_2. *Nat. Catal.* **2022**, *5*, 832−838. (b) Chen, L.; Qu, Q.; Ran, C. K.; Wang, W.; Zhang, W.; He, Y.; Liao, L. L.; Ye, J. H.; Yu, D. G. Photocatalytic Carboxylation of C-N Bonds in Cyclic Amines with CO_2 by Consecutive Visible-Light-Induced Electron Transfer. *Angew. Chem., Int. Ed.* **2023**, *62*, No. e202217918.

(9) Targos, K.; Williams, O. P.; Wickens, Z. K. Unveiling Potent Photooxidation Behavior of Catalytic Photoreductants. *J. Am. Chem. Soc.* **2021**, *143*, 4125−4132.

(10) Cole, J. P.; Chen, D.-F.; Kudisch, M.; Pearson, R. M.; Lim, C.-H.; Miyake, G. M. Organocatalyzed Birch Reduction Driven by Visible Light. *J. Am. Chem. Soc.* **2020**, *142*, 13573−13581.

(11) Soika, J.; McLaughlin, C.; Neveselý, T.; Daniliuc, C. G.; Molloy, J. J.; Gilmour, R. Organophotocatalytic N−O Bond Cleavage of Weinreb Amides: Mechanism-Guided Evolution of a PET to ConPET Platform. *ACS Catal.* **2022**, *12*, 10047−10056.

(12) (a) Glaser, F.; Kerzig, C.; Wenger, O. S. Multi-Photon Excitation in Photoredox Catalysis: Concepts, Applications, Methods. *Angew. Chem., Int. Ed.* **2020**, *59*, 10266−10284. (b) Lepori, M.; Schmid, S.; Barham, J. P. Photoredox catalysis harvesting multiple photon or electrochemical energies. *Beilstein J. Org. Chem.* **2023**, *19*, 1055−1145.

(13) (a) Gosztola, D.; Niemczyk, M. P.; Svec, W.; Lukas, A. S.; Wasielewski, M. R. Excited Doublet States of Electrochemically Generated Aromatic Imide and Diimide Radical Anions. *J. Phys. Chem. A* **2000**, *104*, 6545−6551. (b) Beckwith, J. S.; Aster, A.; Vauthey, E. The excited-state dynamics of the radical anions of cyanoanthracenes. *Phys. Chem. Chem. Phys.* **2021**, *24*, 568−577. (c) Jeong, D. Y.; Lee, D. S.; Lee, H. L.; Nah, S.; Lee, J. Y.; Cho, E. J.; You, Y. Evidence and Governing Factors of the Radical-Ion Photoredox Catalysis. *ACS Catal.* **2022**, *12*, 6047−6059.

(14) (a) Christensen, J. A.; Phelan, B. T.; Chaudhuri, S.; Acharya, A.; Batista, V. S.; Wasielewski, M. R. Phenothiazine Radical Cation Excited States as Super-oxidants for Energy-Demanding Reactions. *J. Am. Chem. Soc.* **2018**, *140*, 5290−5299. (b) Kumar, A.; Malevich, P.; Mewes, L.; Wu, S.; Barham, J. P.; Hauer, J. Transient absorption spectroscopy based on uncompressed hollow core fiber white light proves pre-association between a radical ion photocatalyst and substrate. *J. Chem. Phys.* **2023**, *158*, 144201.

(15) Schmalzbauer, M.; Marcon, M.; König, B. Excited State Anions in Organic Transformations. *Angew. Chem., Int. Ed.* **2021**, *60*, 6270−6292.

(16) (a) Rieth, A. J.; Gonzalez, M. I.; Kudisch, B.; Nava, M.; Nocera, D. G. How Radical Are "Radical" Photocatalysts? A Closed-Shell Meisenheimer Complex Is Identified as a Super-Reducing Photoreagent. *J. Am. Chem. Soc.* **2021**, *143*, 14352−14359. (b) Li, H.; Wenger, O. S. Photophysics of Perylene Diimide Dianions and Their Application in Photoredox Catalysis. *Angew. Chem., Int. Ed.* **2022**, *61*, No. e202110491.

(17) Kang, W.-J.; Li, B.; Duan, M.; Pan, G.; Sun, W.; Ding, A.; Zhang, Y.; Houk, K. N.; Guo, H. Discovery of a Thioxanthone−TfOH Complex as a Photoredox Catalyst for Hydrogenation of Alkenes Using *p*-Xylene as both Electron and Hydrogen Sources. *Angew. Chem., Int. Ed.* **2022**, *61*, No. e202211562.

(18) Day, C. S.; Rentería-Gómez, Á.; Ton, S. J.; Gogoi, A. R.; Gutierrez, O.; Martin, R. Elucidating electron-transfer events in polypyridine nickel complexes for reductive coupling reactions. *Nat. Catal.* **2023**, *6*, 244−253.

(19) Sharma, N.; Zou, H. B.; Lee, Y. M.; Fukuzumi, S.; Nam, W. A Mononuclear Non-Heme Manganese(III)-Aqua Complex in Oxygen Atom Transfer Reactions via Electron Transfer. *J. Am. Chem. Soc.* **2021**, *143*, 1521−1528.

(20) Yan, Y.; Zhou, P.; Rotella, D. P.; Feenstra, R.; Kruse, C. G.; Reinders, J.-H.; Neut, M. v. d.; Lai, M.; Zhang, J.; Kowal, D. M.; Carrick, T.; Marquis, K. L.; Pausch, M. H.; Robichaud, A. J. Potent dihydroquinolinone dopamine D_2 partial agonist/serotonin reuptake inhibitors for the treatment of schizophrenia. *Bioorg. Med. Chem. Lett.* **2010**, *20*, 2983−2986.

https://doi.org/10.1021/acscatal.3c03972
ACS Catal. 2023, 13, 13588−13596